DETERMINATION OF LUNAR SURFACE AGE DATING USING HYBRID POLARIMETRIC RADAR DATA

Kedovikho Yhoshü[1], P.K. Champati Ray[2] and R.S. Chatterjee[2]
[1] Department of Geography,
Nagaland University, Lumami, Nagaland-798627
Email: kedovikho@gmail.com
[2] Indian Institute of Remote Sensing,
ISRO, 4 Kalida road,
Dehradun-248001, India
Email:Champati_ray.iirs.gov.in
Email:rschatterjee.iirs.gov.in

KEYWORDS: Mini-SAR, CSFD, CPR, North Polar.

ABSTRACT: The polar surfaces of the lunar region are in permanent shadow which hinders the study of the lunar region using optical sensors. Mini-SAR, a hybrid radar sensor has the ability to map the permanent shadowed Polar Regions. Miniature synthetic aperture radar (Mini-SAR) a hybrid polarimetric radar uses single frequency S-band which allows the determination of the Stokes parameter. The Stokes parameter help in understanding the surface scattering of the lunar surface based on its surface geometry. The study area is based on selected North Polar Region of the lunar surface. Planetary craters are important for determining the surface age as the craters are well preserved due to less erosion activities. Crater count not only gives surface age but also the geologic processes, impact mechanism and its stratigraphy. For the determination of the surface age, the method applied was crater size frequency distribution (CSFD) based on production function and chronology function. However, certain anomalies like secondary craters have to be removed for age determination. The secondary craters were distinguished on the polarimetric dataset based on its shape as well as its surface roughness. The surface roughness for secondary crater detection was based on the same sense (SC) and circular polarization ratio (CPR) derived from the Stokes parameter. The detected secondary craters were removed and excluded for calibration to improve surface age determination. The age determined after secondary crater correction in the North Polar Region of lunar was 3.99-4.25 Gyr.

1. INTRODUCTION

The morphology of lunar surface is marked by impact craters, grabens and wrinkle ridges. Impact craters are resultants of meteorite bombardment intense during the Heavy Bombardment period. Impact craters are identified as primary and secondary craters based on cratering process. Primary craters are formed from direct meteorite impact whereas secondary are formed from the primary crater ejecta impact on lunar surface. Identification of primary and secondary craters is therefore important for determining the age of the lunar surface. Physical morphology of primary and secondary craters is differentiated based on their outward appearance and surface characteristics.

Bart and Melosh, 2007 distinguished secondary craters based on the study that secondary craters produce larger ejecta fragments at a given crater size than primary craters. The distribution and number of secondary craters and their effect on the crater size frequency distribution was distinguished by Senthil et al., 2011 in which secondary craters form low impact ejecta was identified based on the presence of central mound in the craters. The morphology of crater rim based on observation from specular and diffuse scattering in the crater ejecta was used by Wells et al., 2010 to distinguish between primary and secondary craters on lunar surface. Planetary studies have strengthened with the usage of radar. The advantage of radar in lunar planetary science is its ability to map region in permanent shadowed region (lunar poles) and surface penetrating capability.

Earlier numerical study on cratering production function appears to have been that of Young (1940) in (Neukum, Ivanov and Hartmann, 2001) who gave a value for the slope of production function lines as -2.5. Brown in (Neukum, Ivanov and Hartmann, 2001) also analysed the crudest data on log-log asteroid and meteorite size distribution and fitted straight lines to the data sets, the straight lines on plots of log N vs. log D were named Power law. The use of Power laws in cratering and asteroid fragmentation work became clear when Hartman, 1969 showed experimentally and empirically that power law segments gave good fits, often over two or three orders of magnitude in diameter. The production

function based on the concept of power law size distribution (Neukum, Ivanov and Hartmann, 2001) has the form-

$$N = kD^{-b} \quad (1)$$

Where,
N= cumulative number of craters of diameter ≥ D,
k is constant depending on the definition of N used,
b is power law exponent or slope of the log N vs. log D plot.

Surface age dating based on Crater Size frequency Distribution (CSFD) technique represent the number of craters within a specified region for generating CSFD curve. The age determination for the lunar surface is based on two age function-

a) Production function- It depends on how many craters of a given size are formed in relation to the number of any size (Neukum, Ivanov and Hartmann, 2001).
b) Chronology function- The empirical relationship between the crater frequency plotted versus the radiometric ages.

2. STUDY AREA

Three sites from Lunar North Pole Region was selected. The selenographic locations of the sites are shown (Table 1).

Table 1. Location of the test sites with its central Selenographic latitude and longitude.

Test Site	Description Location(Crater)	Lunar Coordinates	
		Latitude	Longitude
1	Near Preary Crater (Nearside)	87.6	52.7
2	Near Sylvester N Crater (Nearside)	83.6	-45.2
3	Near Wiechert J Crater (Farside)	-87.9	-162.1

3. DATASET

MiniSAR, a hybrid polarimetric dataset was launched on November 2008 onboard Chandrayaan I mission with a wavelength of 12.6 cm in S-band band width.MiniSAR mapped over 95% of the Lunar Polar Regions from February to April 2009 at 150 m resolution (Spudis et al., 2010). Mini-SAR data contains two intensity images H and V and two cross power intensity images between the H and V received, it exhibit hybrid-polarity SAR where the transmitted field is circularly polarized, and the resulting backscatter is received in two mutually coherent linear polarizations (Raney,2006)

The four channel bands of MiniSAR are processed to generate the Stokes parameter (Mohan, Das, and Chakraborty, 2011) given in following equation 2.

$$\left.\begin{aligned} S_1 &= \langle |LH|^2 + |LV|^2 \rangle \\ S_2 &= \langle |LH|^2 - |LV|^2 \rangle \\ S_3 &= 2\,\mathrm{Re}\langle LH.LV^* \rangle \\ S_4 &= -2\,\mathrm{Im}\langle LH.LV^* \rangle \end{aligned}\right\} \quad (2)$$

Where, S_1, S_2, S_3 and S_4 are the Stoke's parameter which represent the horizontal and vertical intensity images and the real and imaginary images hybrid Polarimetric data of MiniSAR.

4. METHODOLOGY

MiniSAR four channel bands are converted into Stokes parameter to derive the Daughter by-products. The narrow strips of MiniSAR data are first co-registered and geo-coded. The geo-coded strips were

then processed to generate the Stokes' products. A relative phase (δ) shift of 45° was observed (Mohan, Das, and Chakraborty, 2011) in MiniSAR, so the phase correction was carried out in order that the data can be reduced in volume in any operational SAR correlator with no prior knowledge of the condition of the surface (Zebker and Lou, 1990). The daughter products are generated from the Stokes' parameter to form various products like surface backscatter, volume backscatter, double-bounce backscatter, LH backscatter and LV backscatter. Circular Polarization ratio (CPR) is an important product generated from the Stokes parameter. CPR is an important surface characterization parameter which helps to differentiate the fresh ejecta formed by primary impact from the secondary impact by the asymmetry pattern of the ejecta. These character of CPR helps in detecting primary from secondary craters.

4.1 Image enhancement and fusion for crater detection

The determination of the impact crater age from MiniSAR data depend on the precise crater attribute extraction. Various algorithms were applied for crater attributes measurement. Crater boundary was enhanced for better boundary demarcation by applying various filters and image transformation algorithms. Surface, volume, double-bounce scatter and LH as well as LV backscatter were stacked and adaptive filter was applied to improve image sharpness and details. The images were transformed by linear transformation- Minimum Noise Fraction (MNF) to determine the inherent dimensionality. MNF maximises the signal-to-noise ratio and order images in terms of decreasing image quality in lower order components (Green et al., 1998).

4.2 Crater counting

Impact craters were counted for determining the age of the lunar surface. Surface age dating technique is based on the concept that the observed crater size frequency distribution (CSFD) of a given surface unit of a known crater production function (PF) and to use the crater frequency for certain crater sizes together with a calibrating chronology function (CF) to obtain an absolute age (Michael and Neukum, 2010).

In the present study, Crater counting method is based on semi-automated technique. Homogenous areas are considered for digitization process- impact craters diameter and the measurement area where the digitized areas are projected into Stereographic map projection defined by the latitude and longitude of the centre point of the circle. The workflow of semi-automated crater attribute (Cratertools) is separated into two processes. The first process deals with the determination of correct sizes of homogeneously cratered measured areas. The second process involves digitization of impact craters and determination of their correct diameters (Michael and Neukum, 2010).

4.3 Secondary crater detection

Detection of secondary craters was done based on their shape, patterns and distribution pattern like clustering and ellipticities. However, the shape alone cannot account for detecting secondary craters as with the increase in distance from the impact site, the hypervelocity impact from which secondary craters have formed enable the secondary craters closely similar to primary craters due to increase in speed of the projectiles (Wells et al., 2010). To detect the subtle differences, CPR and SC images are used. The SC image gives the subsurface scattering from which the surface characteristics can be interpreted. Fresh ejecta and rough surfaces have higher CPR value due to their roughness. Secondary craters that are formed from primary impact debris have asymmetric ejecta blanket which can be used to differentiate the secondary from the primary by studying the CPR and SC images (Yhoshü et al., 2016). In figure 1, it shows the signature of secondary crater and primary crater on SC and CPR image. The secondary craters are more rough due to its freshness emitting lighter tone in SC (Figure 1(b)) and CPR images. Primary crater due to its longer exposure emits darker tone (Figure 1(c)). The secondary craters from which besides the crater roughness, the crater ejecta emitted determines the identification of the secondary craters from primary craters.

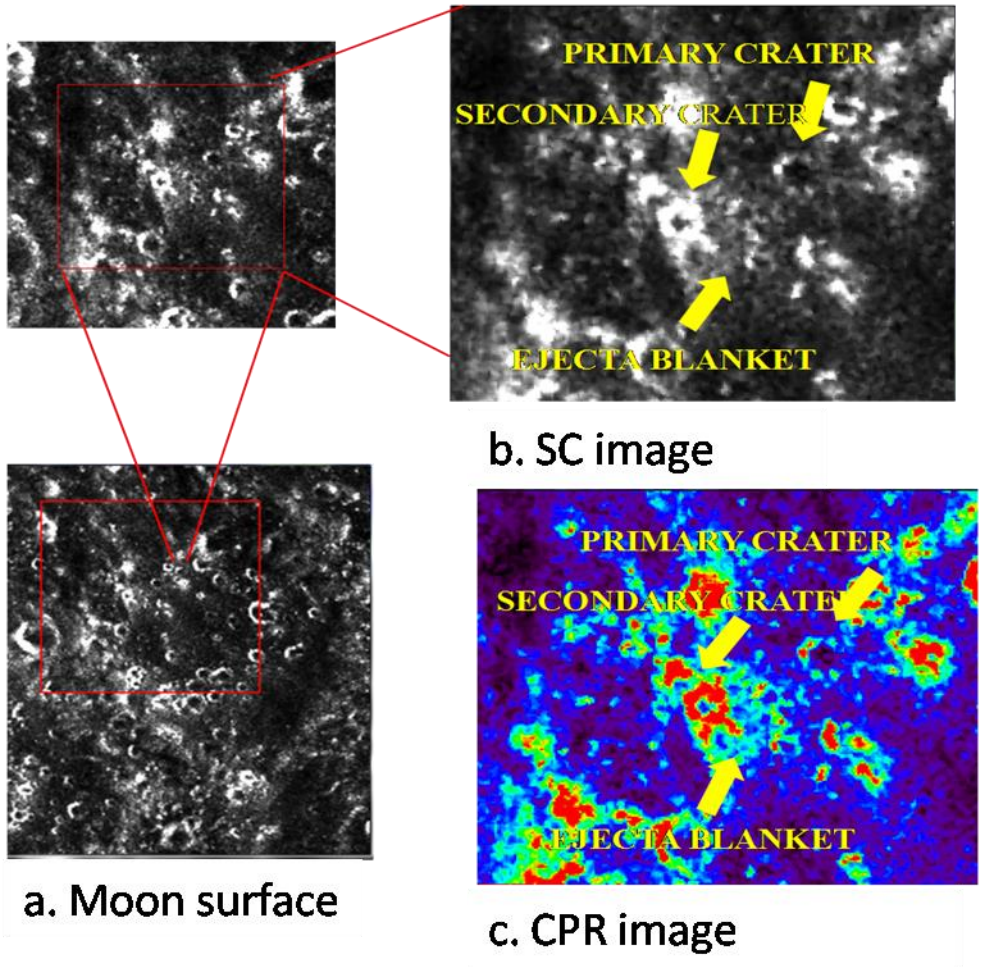

Figure 1. a). moon surface. b). Primary and secondary craters on SC image. c). Primary and secondary craters on CPR image (Yhoshü et al., 2016).

5. AGE DATING

The age of the lunar surface based on the stratigraphy was discussed by earlier workers like Hiesenger et al., 2000. The lunar stratigraphy is divided into five geologic system based on the lunar impact event during the Heavy Bombardment. The five systems are; Pre-Nectarian system(4533-3920 million years), Nectarian system (3920-3850 million years), Imbrian system subdivided into Late Imbrian (3800-3200 million years) and early Imbrian (3850-3800 million years), Erathosthenian system (3200-1100 million years) andCopernician system (1100 million years to the present age).

The production function for the age chronology is based on Neukum production function, a Universal polynomial production function size distribution which abandons the fitting of straight lines power law segments on the log-log plots and introduced non-power law approach for the Lunar Chronology by fitting a polynomial curve to the data (Neukum, Ivanov, and Hartmann, 2001). The craters detected are binned according to their diameter where the time period is expressed by the equation (3) and is valid for diameter range from 0.001 to 300 km.

$$log_{10}(N) = \sum_{j=0}^{11} a_j \times [log_{10}(D)]^j \quad (3)$$

Where,
D is in km,
N is the number of craters per km^2 per Gyr,
and the coefficient a_j are predefined.

6. CONCLUSION

Lunar surface age for test site 1 is shown in Figure 2(a) where the cumulative frequency after secondary crater correction is 4.24 Gyr. The lunar surface age for test site 2 is shown in Figure 2(b) where the crater frequency of the craters after removing the anomalies is 3.99Gyr. Lunar surface age

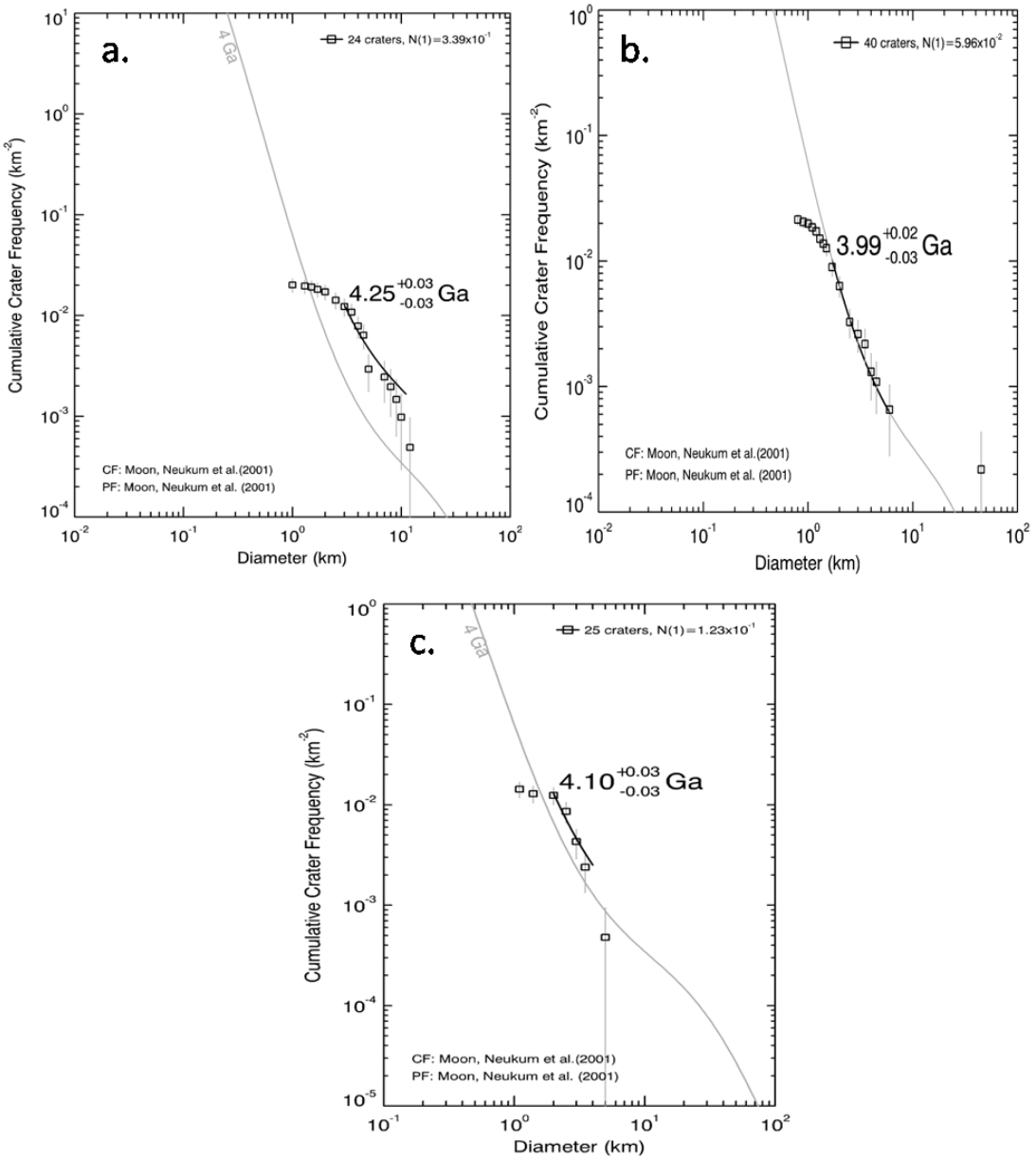

Figure 2. Age Dating by crater attribute in the Three Test Sites. a). Near Peary crater (test site 1) is 4.25 Gyr. b). Near Sylvester N crater (test site 2) is 3.99 Gyr. c). Near Wiechert J crater (test site 3) is 4.10 Gyr.

for test site 3 shown in Figure 2(c) is 4.10 Gyr. The age is determined from semi automated method-Cratertool and production plot from Craterstats is self-calibrated and validated with the Chronology production determined from the samples brought back by the Apollo missions. Additionally, the lunar surface in the present study has been compared to the USGS broad based stratigraphy age produced by Lucchitta, 1978.

The determined age was found to be in accordance with the provided USGS lunar topographic map. The determined age has been improved after removing the anomalies present on the surface. The range of the determined age is 3.99 to 4.25 Gyr from semi-automated precise crater attribute and the USGS

stratigraphy map ranges from 3.20 to 4.53 Gyr in the North Pole region. The age determined from CSFD techniques for the three test sites accounts for 24 crater count for 4,25 Gyr in test site 1, 40 crater count for 3.99 Gyr in test site 2 and for test site 3 it accounts for 25 crater count for 4.10 Gyr (Table 2).

Table2. CSFD based age obtained from Cratertools with crater frequency and its corresponding age in USGS map.

TEST SITE	CRATERTOOL	USGS MAP	CRATER FREQUENCY
1	4.25 Gyr	3.20-4.53 Gyr	24
2	3.99 Gyr	3.20-4.53 Gyr	40
3	4.10 Gyr	3.92-4.53 Gyr	25

.

Reference

Bart, G.D. and Melosh, H.J.,2007. Using lunar boulders to distinguish primary from distant secondary impact craters. Geophysical Research Letter, 34, pp. 1-5.

Hartmann, W.K., 1969, Terrestrial, Lunar and Interplanetary Rock Fragmentation. Icarus, 10 (201), pp.201-213.

Hiesinger, H., Jaumann, R., Neukum G and Head, J.W., 2000. Ages of Mare basalts on the Lunar nearside. Journal of Geophysical Research, 105,(12), pp. 239-275.

Lucchitta, B.K., 1978, Geologic map of the north side of the Moon. Department of the interior United States Geologic Survey (USGS). Interior Geological Survey, Reston, VA-1978-G77061.

Michael, G.G and Neukum, G., 2010, Planetary surface dating from crater size frequency distribution measurements: Partial resurfacing events and statistical age uncertainty. Earth and planetary Science Letters, 294, pp. 223-229.

Mohan, S., Das, A. and Chakraborty, M., 2011. Studies of polarimetric properties of lunar surface using MiniSAR data, Current Science, 101(2), pp.159-164.

Neukum, G., Ivanov, A. and Hartmann, W.K., 2001. Cratering records in the inner Solar System in relation to the Lunar reference system. Space Science Review, 96, pp.55-86.

Neish, S. Nozette, S. Nylund, M. Palsetia, W. Patterson, M.S. Robinson, R.K. Raney, R.C. Schulze, H. Sequeira, J.Skura, T.W. Thompson, B.J. Thomson, E.A. Ustinov and Winters H.L.,2010. Initial results for the North pole of the Moon from MiniSAR, Chandrayaan 1 mission, Geophysical Research Letter, 37, pp.1-6.

Patterson, G.W., Bussey, D.B.J., Spudis, P.D., Neish,C.D., Thomson, B.J., Carter, L.M.,

Raney, R. K., 2006. Dual-Polarized SAR and Stokes Parameters, IEEE Geoscience and Remote Sensing Letters, 3(3), pp. 317-319.

Spudis, P.D., D.B. Bussey, S.M. Baloga, B.J. Butler, D.Carl, L.M. Carter, R.C. Elphic, J.J. Gillis-Davis, J.N. Goswami, E.Heggy, M. Hillyard, R. Jensen, R.L. kirk, D. La Vallee, P.McKerracher, C.D.

Senthil, K. P., Kumar, A.S., Keerthi, V., Goswami, J.N., Khrishna, B.G. and Kumar, A.S.K., 2011. Chandrayaan-1 observation of distant secondary craters of Copernicus exhibiting central mound morphology: Evidences for low velocity impacts on the Moon. Planet Space Science, pp. 870-879.

Wells, K. S., D. B. Campbell, B. A. Campbell, and Carter L. M., 2010. Detection of small lunar secondary craters in circular polarization ratio radar images, Journal of Geophysical Research, 115, pp. 1-10.

Yhoshü, K., Chatterjee, R.S and Champati Ray, P.K., 2016. Secondary crater detection from Mini-SAR for lunar surface age dating. Current Science,110(3), pp. 304-306.

Zebker, H.A. and Lou, Y., 1990. Phase calibration of imaging radar polarimeter stokes matrices, IEEE transaction of Geoscience and remote sensing, 28(2), pp.246-252.